Materials and Structures (2024)57:243
https://doi.org/10.1617/s11527-024-02477-w

ORIGINAL ARTICLE

Corrosion attack in existing reinforced concrete structures: in-field investigation and analysis of naturally corroded bars

Casprini Elena · Passoni Chiara · Bartoli Gianni · Marini Alessandra

Received: 31 May 2024 / Accepted: 20 September 2024

Abstract Corrosion of steel bars is a major issue for the management of existing reinforced concrete structures, since affecting many ageing structures and infrastructures and introducing risk for safety and reliability, as well as high maintenance costs. Intervention strategies should be planned and carried out according to the effective state of deterioration and to the expected evolution of performances over time. The critical parameters needed to evaluate these performances are the intensity and pattern of the corrosion attack, referring to both extension and depth of the attack. However, this information is rarely available and hard to predict when dealing with real structures. This paper presents a field investigation on existing corroded structures characterized by different environmental conditions. Corroded bars were removed from structural elements, the corrosion patterns were studied, and then the bars were tested to determine their mechanical properties. The objective of this study is to increase the knowledge of the effects of corrosion in natural environments and to propose a method to relate easy-measurable environmental conditions with the characteristics of the expected corrosion attack, which need to be further validated.

Keywords Corrosion effects · Existing reinforced concrete structures · Durability · Structural diagnosis and assessment

C. Elena (✉) · P. Chiara · M. Alessandra
Department of Engineering and Applied Sciences, University of Bergamo, Viale Marconi 5, 24044 Dalmine, Italy
e-mail: elena.casprini@unibg.it

B. Gianni
Department of Civil and Environmental Engineering, University of Florence, Via di S. Marta 3, 50139 Florence, Italy

1 Introduction

When dealing with existing reinforced concrete (RC) structures, the proper evaluation of structural performances over time and the selection of intervention strategy should necessarily consider the effects of corrosion, since they can lead to a reduction in strength, stiffness and ductility of RC structural members [1]. The main effects of corrosion on RC structures can be the longitudinal and transversal bars cross-section reduction, the concrete cracking and spalling due to oxide expansion, and consequent possible bond strength reduction or buckling of longitudinal rebars in compression. Although many studies deal with the investigation of these effects on the structural behaviour of RC structures [2, 3], such results are rarely considered in the common practice.

In this perspective, the DEMSA protocol (Deterioration Effect Modelling for Structural Assessment) has been proposed by the authors [4]. It provides a

simplified procedure for preliminary detection, evaluation, and modelling of corrosion effects for the evaluation of structural performances in practical applications. In the DEMSA protocol, a relationship was established between easy-measurable environmental and aggressiveness conditions (grouped into four different Corrosion Risk Scenarios, CRS) and the main characteristics of the corrosion attack (such as the average corrosion rate, i.e. the rate of penetration of the corrosion attack into the reinforcing bars, and the ratio of maximum to average attack). The description of the corrosion attack would then allow calibrating simplified equivalent damage parameters (EDPs), such as the average and minimum residual cross-section of the bars, the reduced compressive strength of cracked concrete surrounding the bar, the modified stress–strain relationship of steel and the reduced bond strength between steel and concrete. These parameters can be then implemented in the structural models available in the literature in order to evaluate whether corrosion effects could be relevant for the structural response; the authors showed an example of models calibration in Casprini et al., 2022 [5].

Nevertheless, the applicability of this protocol and other methods [6–8] in structural assessment analyses is still limited due to the lack of data related to the expected corrosion attack characteristics in natural environments, which is the fundamental information to calibrate the models. Due to the difficulty in identifying the actual corrosion pattern on the bars embedded in the concrete, most available data on corrosion patterns thus come from experimental laboratory campaigns on modern bars. However, unlike natural corrosion in existing structures, which is a "slow" process that develops over the years, very high corrosion current density is often applied for short periods of time in artificial corrosion to both represent the same level of corrosion as in existing structures and to obtain results within a reasonable time frame. Typical values of corrosion current density used in experimental campaigns range between 80 and 10000 $\mu A/cm^2$, while in nature values of corrosion rates higher than 10 $\mu A/cm^2$ are rarely measured and the most common values are between 0.01 and 1 $\mu A/cm^2$ [9]. Moreover, the presence of concrete surrounding the bar leads to uneven and hardly predictable attack patterns even within the same bar. The effects of corrosion in terms of intensity and pattern of the attack can thus be significantly different in artificial and natural corrosion processes. Some experimental campaigns simulated corrosion processes without applying current to structural elements, as for example the long-term program carried out at Laboratoire Matériaux et Durabilité des Constructions in Toulouse [3], where RC beams have been exposed to chloride contaminated environments for several years (up to 40 years), simultaneously with applied loads; other researchers simulated natural corrosion exposure on concrete samples with embedded bars through wet-dry cycles in water solution containing chlorides (5–17% of NaCl concentration) for time periods ranging between 280 days and 3 years [10, 11]; finally, in other experimental campaigns, to maintain lower values of concrete current density (200 ÷ 250 $\mu A/cm^2$), specimens are cast by adding chlorides in the mixing water or stored in saline solutions [2].

In this research, a field investigation on four existing deteriorated RC buildings characterised by different Corrosion Risk Scenarios was carried out. For each building, a few bars were extracted and characterised in terms of corrosion pattern and mechanical properties. The following sections summarize the steps of the experimental program performed on each structure analysed:

- Corrosion Risk Scenario (CRS) identification according to the DEMSA protocol procedure [4];
- Analysis of the corrosion attack pattern (penetration and distribution along the bar length) through computerized tomographic scans on bars extracted from the investigated structural elements;
- Definition of the actual corrosion attack characteristics (based on measured data) and comparison with the expected ones (based on CRS, following the DEMSA protocol procedure);
- Evaluation of the residual mechanical properties of the bars in relation to the corrosion pattern by tensile tests.

2 In-field investigation: buildings description and CRS identification

Few data on the corrosion attack characteristics of naturally corroded bars removed from existing structures can be found in the literature, mainly connected

to bridges [12]. The best-known examples are the *Dickson Street* overpass in Montreal, which was demolished after only 40 years of operation, and the *Stallbaka* bridge in Sweden [13, 14]. Even fewer data are available for existing RC buildings, especially those typical of the post-world-war II European heritage, which are indeed of primary interest because of the urgency to define strategies for their renovation [15, 16]. For these case studies, data from experimental laboratory campaigns are often not suitable also because they usually refer to ribbed bars rather than smooth bars typical of this period.

2.1 Case-studies description

In the present study, the in-field investigations were carried out on existing buildings built between the Sixties and the Nineties all presenting damage due to corrosion and exposed to different environmental conditions, thus belonging to different Corrosion Risk Scenarios (CRS; [4]). All the buildings are located in Northern Italy and all the studied structural systems are cast-in-place or precast RC frames (details of the buildings' features may be found in Casprini, 2021 [17]). Information on the final use and type of the buildings, construction year, the damaged structural elements and type of damage observed during the visual inspection carried out in 2020 are collated in Table 1, together with the labels assigned to the bar samples. A representation of all the sampled bars is reported in Appendix 1.

Some information was gathered about the buildings' history to better understand the exposure conditions. About the abandoned building (AB), the portion of the roof above the external colonnade, where the damaged beam of interest is located, collapsed in 2006, along with the guttering. The elements in the area below were then exposed to frequent stagnations of water during rainy periods. One of these beams was thus examined and a bar sample (total length of 2.2 m) was extracted from the bottom layer of reinforcement in the central part of the beam, and then divided in three samples (AB2-3-4); the data were compared to the ones of an adjacent beam, which was instead still sheltered from rain (bar AB1, from the central portion of the sound beam). The former showed rust stains, longitudinal and transverse cracks, concrete cover spalling and internal delamination between the bars and the concrete cover preventing water from drying out (Fig. 1a); the latter did not show any external signs of damage. The car park annexed to a residential building (RB) suffered water infiltration from the garden above since construction. On the first beam examined (corresponding to bar RB1, sampled from the bottom layer of reinforcement), an additional layer of high-strength mortar had been applied to the concrete surface during past repair works, probably to protect the corroding beams: a large area of internal delamination was detected between such mortar layer and the pre-existing concrete (Fig. 1b). The additional layer may have prevented the water in contact with the reinforcing bars to progressively dry out. Despite the presence of a large amount of corrosion products on

Table 1 Characteristics of the investigated buildings and observed signs of damage

Type of building	Year of construction	Bar provenance element	Corrosion-induced deterioration	Bar Sample
Abandoned construction, formerly used as a nursing home for elderly people	1960	Sound beam	No	AB1
		Deteriorated beam	Delamination	AB2-3-4
Annexed private car park in a residential building	1970	Beam 1	Delamination	RB1
		Beam 2	Longitudinal cracking	RB2
School	1959	Column 1	Thin crack at the bottom corner	SB1
		Column 2	Thin crack at the bottom corner	SB2
Industrial building	1990	Beam (stirrup)	Spalling – Rust staining	IB1

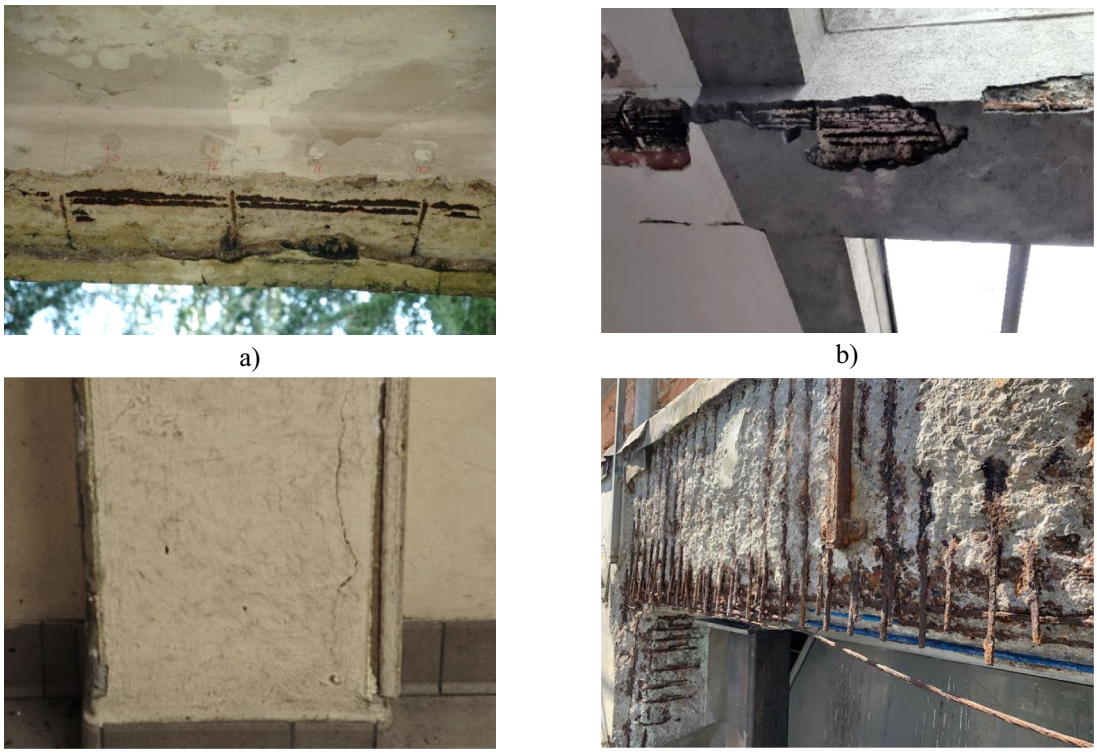

Fig. 1 Visible damage detected in the structural elements of the investigated case study buildings: visible corrosion of the bars exposed after concrete delamination and spalling in the beam AB2-3-4 (**a**) and RB1(**b**), longitudinal cracking at the bottom corner of columns SB1-2 (**c**), corroded stirrups and cover spalling in IB1 (**d**)

the bar surfaces, no longitudinal cracks were visible on the concrete surface. On the second beam (RB2), the concrete surface was not covered with an additional plaster layer, and longitudinal cracking was detected.

In the school building, almost 10% of the RC concrete columns inside the school rooms presented cracks at the bottom corners corresponding to the longitudinal bars (Fig. 1c). Signs of high relative humidity (R.H.) were not found, and the possible contact with water was probably related to the frequent cleaning of the floor; bars SB1 and SB2 were extracted from the bottom corners of two different columns.

Finally, the structural elements of the investigated industrial building are made of precast reinforced concrete and cladded with light metal panels. The building unit has been in operation since 1990. In 2020, a small rust spot was noticed on the metal cladding of an external side beam; the finishing was subsequently removed. The condition of the beam under the finishing is shown in Fig. 1d. In this case, salt leakage from a tank located on the side of the room next to the beam led to chloride-induced corrosion; a stirrup was removed from the side of the damaged beam (bar IB1).

2.2 Corrosion risk scenario identification

After the visual inspection and the detection of visible signs of damage, a Corrosion Risk Scenario (CRS) was associated to each damaged structural element. CRSs are connected to different environmental and aggressiveness conditions that can trigger different corrosion attack types and intensities. In the DEMSA Protocol [4], four different scenarios were identified: absence of condition able to trigger significant corrosion processes (Scenario 0); carbonation-induced corrosion in the presence of wet-dry cycles or high R.H. (Scenario 1); carbonation-induced corrosion in the presence of low chloride content in the cementitious matrix, even with moderate R.H. (Scenario 2); and chloride-induced corrosion (Scenario 3). Within each scenario, different aggressiveness classes (AC)

(from O-ordinary, to H-high, and E-extreme) are also defined, characterised by increasing chloride content and R.H. Some instrumental tests such as chloride content, carbonation depth and cover depth may be required to identify the Scenario of interest: the chloride content is measured through standard chemical titration on concrete samples from the analysed structures [18] while measurements of carbonation depth are carried out using the quick and cost-effective CARBONTEST® method [19].

The proposed Corrosion Risk Scenario identification procedure is represented in Fig. 2 (referring to the application to the beam of the abandoned building AB2-3–4, leading to Scenario 1). The first step consists in examining the possibility of entrance of chlorides from the outside of the concrete (Scenario 3); their presence often entails a high risk of activated significant corrosion processes, also in average humidity conditions. Furthermore, the presence of chlorides in the concrete matrix is evaluated also in case of absence of chlorides in the external environment. Indeed, a low amount of chloride in the matrix ($< 0.4\%$ with respect to cement weight) cannot be excluded a priori in existing structures, since they could have been introduced during the construction phase, through accelerant admixtures based on calcium chloride or contaminated water and aggregates (Scenario 2). Also, in most cases, especially when the attack caused by chlorides is localized (Fig. 1c), the external signs of damage may be less evident than those due to carbonation induced corrosion and presence of water (Fig. 1a); in contrast, the corrosion attack may be more relevant and dangerous.

If chlorides related corrosion is then excluded, the possibility of carbonation-induced corrosion (Scenario 1) is evaluated. In this case, the activation of corrosion is mainly related to carbonation overcoming the concrete cover depth and depassivating the steel bars, therefore the depth-of-carbonation and cover depth measurements should be compared. However, even if bars are depassivated, in absence of frequent contact with water or high R.H., corrosion processes may neither activate nor lead to significant effects on the structure. This is clear from the example related to bar AB1 and bars AB2-3-4 (Fig. 3); in both cases carbonation had already reached the rebar level, but corrosion did not occur in bar AB1, located in a dry beam sheltered from rain. So, the last step of the identification procedure regards the detection of the possible contact with water or the presence of high R.H. The procedure was applied to all the considered cases. The results of the visual inspection and material tests, and consequent selection of the Corrosion Risk

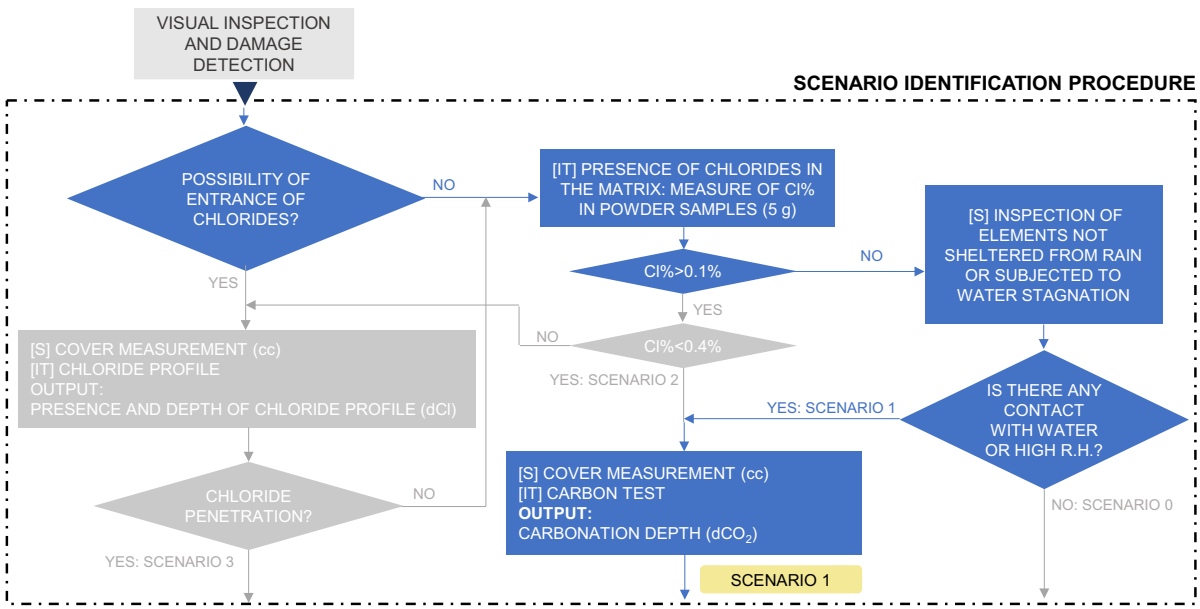

Fig. 2 Example of Scenario Identification for sample AB2-3-4 (adapted from Casprini et al., 2022 [4]); type of action required: [S] survey, [IT] instrumental test

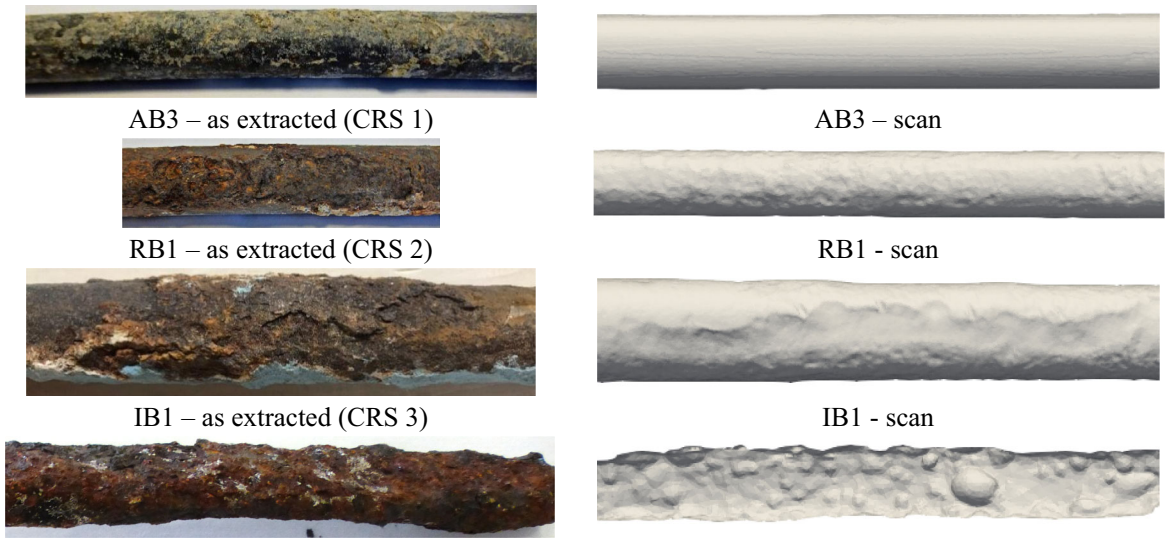

Fig. 3 Details of some portions of the bars, as extracted and by tomographic scan: uncorroded bar AB1, corroded bar AB3, heavily corroded bar RB1 and IB1

Table 2 Corrosion Risk Scenario identification for the examined samples: collected data

Bar #	Exposure condition	cc [mm]	dCO_2 [mm]	$dCO_2 > cc$ Yes/No	Cl quantity [%]/ No	Water contact Type/ No	Scenario–Class
AB1	Outdoor sheltered from rain	20	53	Yes	No	No	0
AB2		25	46	Yes	No	Leakage in the case of rain	1–E
AB3					No		1–E
AB4					No		1–E
RB1	Basement sheltered from rain	15	40	Yes	0.27%	Infiltration	2–H
RB2		15	70	Yes	No	Rare	1–H
SB1	Indoor	35	100	Yes	0.20%	Floor cleaning	2–O
SB2		45	90	Yes	0.34%	Floor cleaning	2–O
IB1	Outdoor with finishing	–	–	n.a	2.5–5%	No	3–E

Scenarios and aggressiveness classes for each specimen are reported in Table 2.

3 Analysis of the corrosion attack on naturally corroded bars

The primary effect of corrosion on a steel bar is the reduction of its cross-section, which entails also a strength reduction. Therefore, the effects of corrosion on the structural behaviour of RC elements may be first considered by modelling a reduced equivalent diameter of the corroded bars [6]. This equivalent diameter may be estimated as a function of two main characteristics describing the corrosion attack, which are the average corrosion rate v_{avg} and the maximum to average attack ratio R_p [4]. Such characteristics depend on the type of corrosion attack and vary for each Corrosion Risk Scenario (CRS). With reference to the case study buildings, which were subjected to different attacks, the corrosion pattern is determined by means of tomographic scans. Then, starting from these measured residual cross-section distributions, the corrosion attack characteristics can be estimated and compared to the reference ranges defined in the

literature for different environmental conditions (here associated with the CRSs).

3.1 Corrosion pattern distribution on corroded bars

After the extraction, the bars were cleaned from corrosion products. Mechanical cleaning through sandblasting, at approximately 5.5 bars of pressure, was preferred to other cleaning methods, such as metallic brushing and acid cleaning, being considered as the most effective and least time-consuming method in removing corrosion products from the bar surfaces [20]. The bars were then measured and weighed to obtain the bar length L_b and mass M_b. The nominal original diameter ϕ_0 was estimated by measurement of non-corroded parts of the bars or from original drawings, and the nominal cross-section A_0 calculated accordingly. The bar surface representation was obtained through Computerized Industrial Tomography scans performed by *TecEurolab*© (detector: flat panel PE XRD 1621 AN 14 ES, maximum resolution 70 μm, pixel pitch 200 μm).

From the tomographic scans, it was possible to observe that, for each specimen, the qualitative corrosion pattern was consistent with the expected one, in relation to the CRSs. The bar AB1, for which Scenario 0 was assumed, was indeed uncorroded (Fig. 3). Also, the bar subjected to carbonation-induced corrosion presented a quite uniform cross-section reduction along the bar segment length and a large amount of corrosion products (AB3 in Fig. 3); bars belonging to Scenario 2 featured localized attacks, either in the pit-shape or extended over a reduced length (as bar RB1 in Fig. 3); finally, bars characterized by chloride-induced corrosion (IB1 in Fig. 3) showed several localized deep attacks and experienced a heavy cross-section reduction. As a matter of fact, an increase of the intensity of the corrosion attack by increasing the Scenario and the aggressiveness class is observed.

The output obtained by the tomographic scans (a mesh describing the surface geometry) were then processed by the software *vmtk* (*The Vascular Modeling toolkit*, [21]), usually adopted for the analysis of blood vessels, to obtain a geometric description of the distribution of the actual residual cross-section along the bar length. The spacing between bar sections was set equal to 1 mm provided that shorter distances did not result in more detailed information. The output of the process is therefore the cross-section measurements A_i at the chosen locations (Fig. 5). Finally, for each specimen, some characteristics of the corrosion pattern, defined in Table 3, were calculated by elaborating the available data; results are reported in Table 4.

The results in terms of average residual cross-section obtained by gravimetric method ($A_{avg,w}$) match very well with those obtained with tomographic scan ($A_{avg,ts}$, Table 4), since, in this investigation, the samples extracted and analysed were subjected to tomographic scan throughout their entire dimension, while in other studies [14], 3D scanning could be performed only on some portions of the bars, and the results compared with the weight loss of the whole bar.

Although the results in Table 4 cannot be generalized due to the limited number of analysed bar samples, they allow identifying some significant parameters to describe the attack distribution along the bar length in relation to the corrosion risk scenario, namely the cross-section range $\Delta A_{ts}/A_{avg,ts}$ and the coefficient of variation *Co.V.* of the corrosion attack distribution. The former highlights the extreme values of the corrosion attack compared to the average residual cross-section and therefore it accounts for both the attack depth and the average residual dimension of the bar. The latter also provides information on the variability of the attack distribution along the bar length. Such parameters assume low values for bars in Scenario 1 ($\Delta A_{ts}/A_{avg,ts} < 10\%$ and $Co.V. < 2\%$), and increase according to the chloride content, which is the main factor controlling the attack variability. Indeed, higher values are found in Scenario 2 ($10\% < \Delta A_{ts}/A_{avg,ts} < 60\%$ and $2\% < Co.V. < 20\%$) and the highest in Scenario 3 ($\Delta A_{ts}/A_{avg,ts} > 60\%$ and Co.V. $> 20\%$). These values, along with the minimum residual cross-section, are reported in Fig. 4, showing that, for the analysed bars, the corrosion attack progressively becomes more variable and intense, when shifting from Scenario 1 to 3.

In the following graphs, the residual cross-section distributions A_i obtained from the tomographic scans are shown (continuous red and green lines in Fig. 5a,b,c,d), along with additional cross-section measurements: the initial section A_0 refers to the assumed original diameter, represented by the solid grey lines, and the inherent tolerances (defined as ± 4.5% with respect to the original section [22]),

Table 3 Geometric characteristics of the corrosion attack on rebars, definition of the parameters

Symbol	Unit	Parameter	Formula or measurement
$m_{l,0}$	g/m	nominal linear mass density	$m_{l,0} = A_0 \cdot \gamma_{steel}$ $\gamma_{steel} = 7850\,kg/m^3$
$m_{l,c}$	g/m	corroded linear mass density	$m_{l,c} = M_b/L_b$
Δm	%	mass loss with respect to the nominal one	$\Delta m = \left[(m_{l,0} - m_{l,c})/m_{l,0}\right] \cdot 100$
$A_{avg,w}$	mm^2	average cross-section by gravimetric method (absolute and percentage of the nominal one)	$A_{avg,w} = A_0 \cdot (1 - \Delta m/100)$
	%		$(A_{avg,w}/A_0) \cdot 100$
$A_{avg,ts}$	mm^2	average cross-section by scan (absolute and percentage of the nominal one)	$A_{avg,ts} = \mathrm{mean}(A_i)$
	%		$(A_{avg,ts}/A_0) \cdot 100$
$A_{min,ts}$	mm^2	minimum cross-section by tomographic scan	$A_{\min,ts} = \min(A_i)$
	%		$(A_{\min,ts}/A_0) \cdot 100$
$A_{max,ts}$	mm^2	maximum cross-section by tomographic scan	$A_{\max,ts} = \max(A_i)$
	%		$(A_{\max,ts}/A_0) \cdot 100$
ΔA_{ts}	mm^2	cross-sections range	$\Delta A_{ts} = A_{\max,ts} - A_{\min,ts}$
$\Delta A_{ts}/A_0$	%	(in percentage of the nominal one)	$(\Delta A_{ts}/A_0) \cdot 100$
$\Delta A_{ts}/A_{avg,ts}$	%	(in percentage of the average one)	$(\Delta A_{ts}/A_{avg,ts}) \cdot 100$
ΔA_{avg}	mm^2	average cross-section reduction	$\Delta A_{avg} = A_0 - A_{avg,ts}$
ΔA_{max}	mm^2	maximum cross-section reduction	$\Delta A_{\max} = A_0 - A_{\min,ts}$
R_{sec}	–	maximum on average attack ratio	$R_{\sec} = \Delta A_{\max}/\Delta A_{avg}$
$st.dev$	mm^2	Standard deviation of scan measures (N = number of measurements)	$st.dev = \sqrt{\frac{1}{N-1} \cdot \sum_{i=1}^{N} (A_i - A_{avg,ts})^2}$
$C.V$	%	Coefficient of variation of scan measures	$C.V. = (st.dev/A_{avg,ts}) \cdot 100$

Table 4 Geometric characteristics of the corrosion attack pattern on the bar samples extracted from the case study buildings (parameters are defined in Table 3)

Bar	ϕ_0 mm	A_0 mm^2	$A_{avg,w}$ mm^2 (%)	$A_{avg,ts}$ mm^2 (%)	$A_{min,ts}$ mm^2 (%)	$A_{max,ts}$ mm^2 (%)	ΔA_{ts} mm	$\frac{\Delta Ats}{A0}$ %	$\frac{\Delta Ats}{A_{avg,ts}}$ %	R_{sec} -	$st.dev$ mm^2	$Co.V$ %
AB2	16	201.1	191.4 (95.2)	191.1 (95.0)	184.1 (91.6)	197.4 (98.2)	13.3	6.6	6.9	1.70	2.44	1.3
AB3			194.4 (96.7)	193.5 (96.3)	187.9 (93.5)	197.3 (98.1)	9.4	4.7	4.9	1.75	1.79	0.9
AB4			190.9 (94.9)	190.7 (94.8)	181.3 (90.2)	197.5 (98.2)	16.2	8.1	8.5	1.90	3.59	1.9
RB1	20	314.2	282.2 (89.8)	285.5 (89.9)	253.2 (80.6)	299.4 (95.3)	46.3	14.7	16.4	1.93	10.95	3.9
RB2	16	201.1	193.7 (96.3)	193.1 (96.1)	190.4 (94.7)	197.6 (98.3)	7.2	3.6	3.7	1.35	1.16	0.6
SB1	10.3	83.3	72.6 (87.2)	72.3 (86.8)	60.2 (72.3)	82.3 (98.8)	22.1	26.5	30.5	2.1	5.08	7.0
SB2	9.8	75.4	63.1 (83.7)	62.8 (83.2)	43.5 (57.4)	75.9 (100)	31.9	42.3	50.8	2.5	10.62	16.9
IB1	10	78.5	42.5	41.9	25.2	59.5	34.2	43.6	81.7	1.45	9.63	23

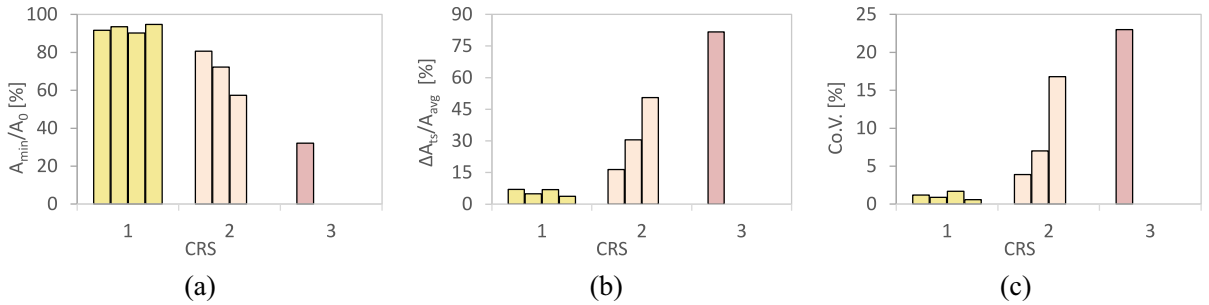

Fig. 4 Values of % minimum cross section A_{min}/A_0 (**a**), cross-section range over the average section (**b**) and of the coefficient of variation (**c**) in different scenarios (S1-S2-S3)

described by the dotted grey lines; the average cross-section by digital scan $A_{avg,ts}$ and the average cross-section obtained by weighing the corroded bar $A_{avg,w}$ (lighter red and green continuous lines), which are always very similar; the maximum A_{max} and minimum A_{min} cross-section measured (light red and green dashed lines), to highlight the extension of the range of the cross-section measurements. The cross-section measurements are grouped together for each structure (in Fig. 5a–d), to emphasize similarities and differences of corrosion patterns in the same structure, which does not always correspond to same aggressiveness conditions.

Some considerations on the corrosion attack pattern in the examined bars can be drawn. The main characteristic of the attack on bars AB2 and AB4 (green and red solid lines in Fig. 5a, respectively) is a fairly uniform cross-section reduction corresponding to 5% of the original cross-section, as expected for Scenario 1, except for two segments of almost 15 cm (over the total length of 220 cm) that present a higher reduction of about 10% (right end of the bar AB2 and centre of the bar AB4). In these regions, the presence of internal delamination at the rebar level could have prevented water from draining out during rain periods, leading to a more sever attack; in this case, the corrosion patterns observed in the two bars (same corrosion risk scenario) have similar characteristics in terms of intensity of the attack and variability of the attack distribution. In building RB (Fig. 5b), the corrosion attack is very different between the two bars extracted from the two selected structural elements, confirming the presence of two different CRSs. Although the higher carbonation depth measured in the beam RB2 may show a higher porosity than beam RB1, and relatively lower quality of the concrete surrounding the bar, the observed attack is much stronger in bar RB1, with a cross-section reduction of approximately 19%. This can be due to the presence of a low chloride content in RB1 (0.27% with respect to cement weight) (Scenario 2); in addition, the hygroscopic nature of chlorides may have contributed in keeping a higher internal humidity in the concrete, leading to a stronger attack.

As for the school building SB (Fig. 5c), several localized deep attacks are present along the bars SB1 and SB2 due to the presence of chloride ions in the cementitious matrix (Scenario 2). More evidently than in the previous buildings, the corrosion attack seems to involve all the bar perimeter, further confirming that chlorides are spread throughout the surrounding concrete. It should be noted that, by carrying out a preliminary survey of the building, neither evident signs of corrosion-induced damage or of aggressive environmental conditions could provide warnings about the actual state of preservation of the reinforced concrete elements. The building was in use, normal indoor R.H. was observed, and only thin cracks were present at the bottom corners of the columns. Despite such a normal environment, a small quantity of chloride ions with respect to cement weight produces a relevant increase in the corrosion in some portions of the reinforcement, with a maximum cross-section reduction of 45%, which is one of the most severe damages detected, also due to the small size of the bars.

Finally, the bar of the industrial building IB1 (Fig. 5d), corroded in a highly chloride contaminated environment (Scenario 3), shows the heaviest and most uneven cross-section reduction, despite being the building the most recently constructed among the analysed case studies. Although the ratio between the

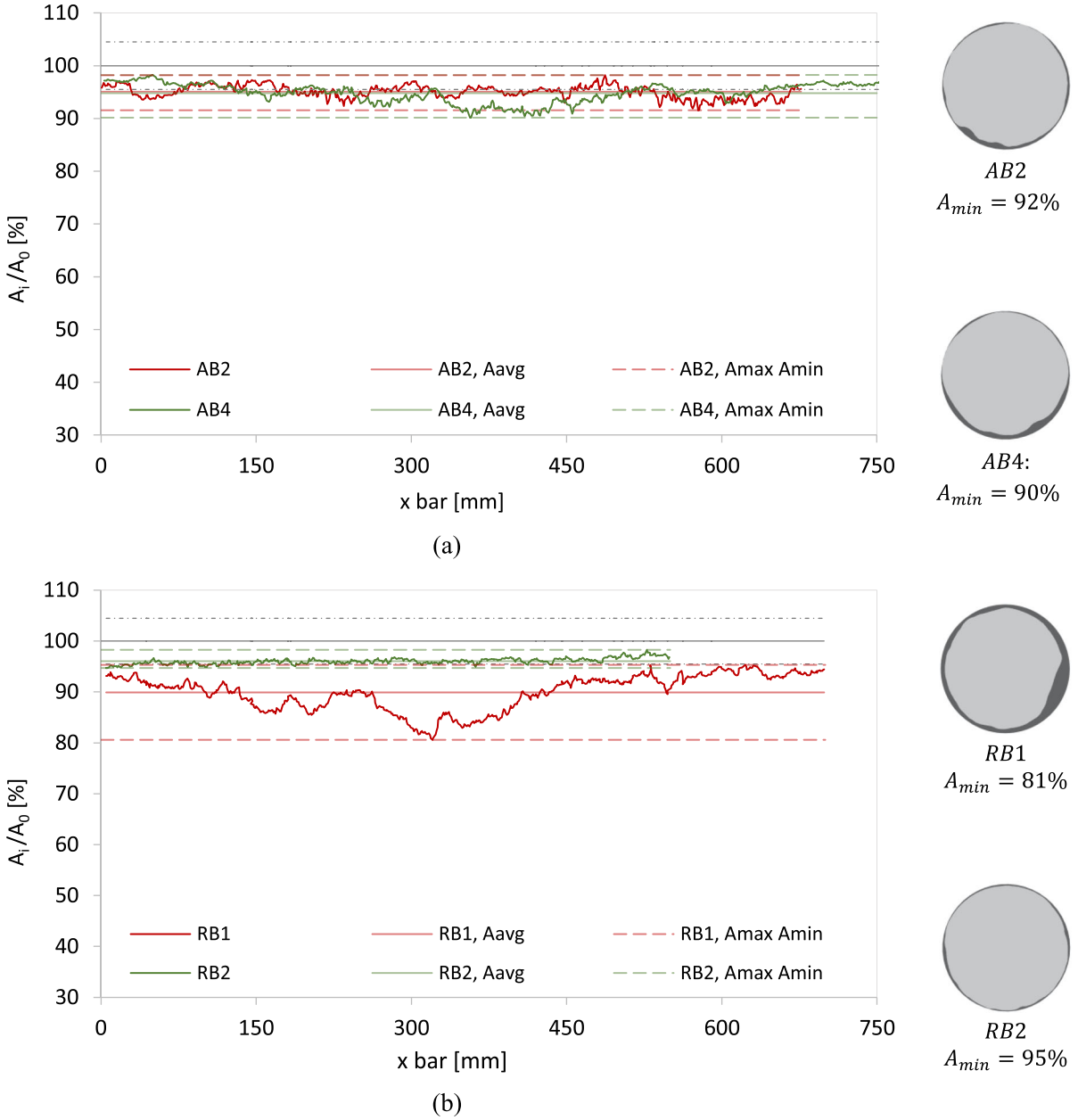

Fig. 5 Residual cross-section distribution for: (**a**) the abandoned building (AB2-AB4), (**b**) the residential building (RB1-RB2), (**c**) the school building (SB1-SB2), and (**d**) the industrial building (IB1) on the left. Examples of the sections obtained in some significant location, on the right. (All bar samples have different total length L_b)

maximum and average corrosion attack was expected to be very high for the specimen in Scenario 3 (values ranging between 4 ÷ 10 are reported in the literature in the case of chloride-induced corrosion), the content of chloride in the concrete surrounding the bar was so high (2.5–5%) as to lead to a widespread intense attack along the whole bar length, reducing drastically also the average residual cross-section and consequently the ratio R_{sec}, which, in this case, resulted equal to 1.45.

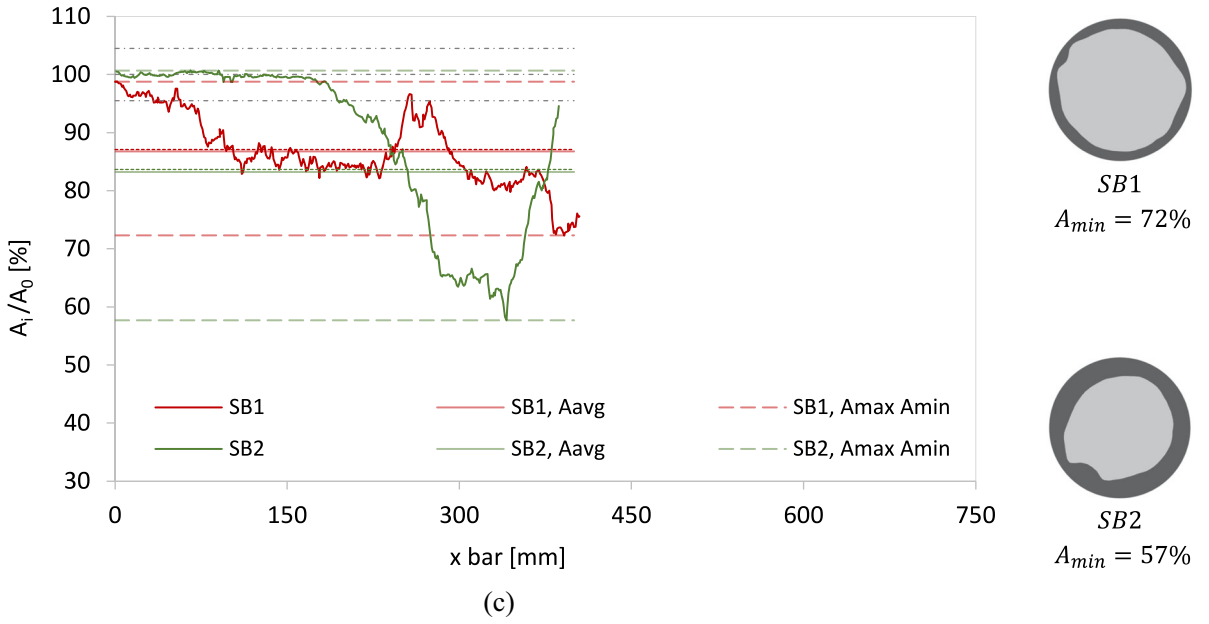

(c)

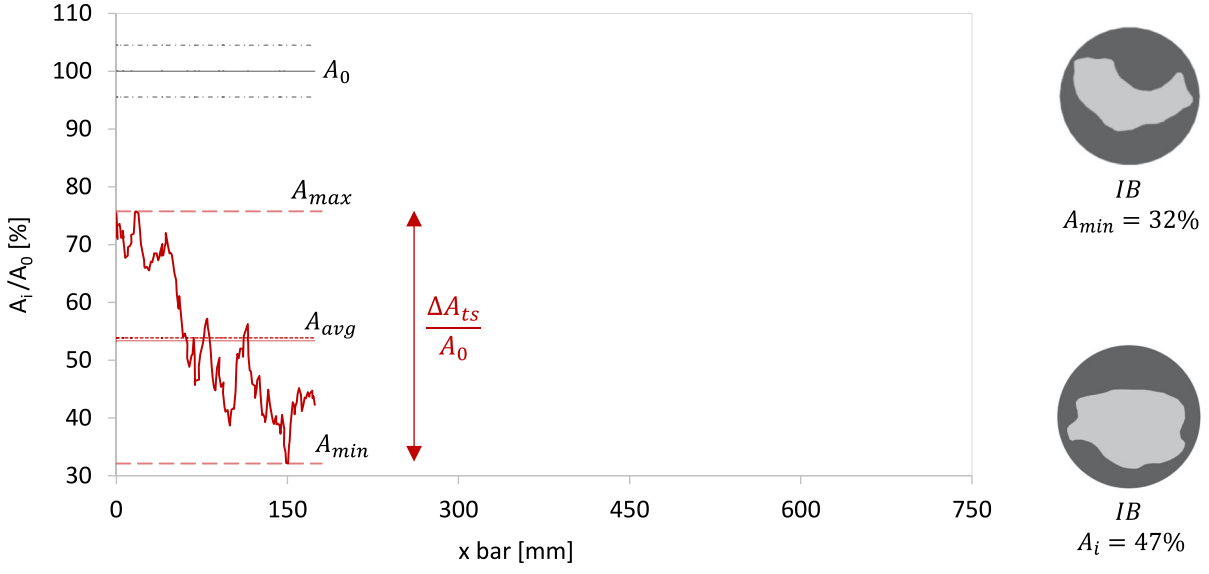

(d)

Fig. 5 continued

3.2 Estimate of the corrosion attack characteristics

Starting from the measured residual cross-section distributions, the main characteristics of the corrosion attack which may have occurred in the buildings were estimated in terms of average corrosion rate v_{avg} and maximum to average attack ratio R_p.

These characteristics of the attack were calculated through the formula expressed in Table 5. First, considering an equivalent regular circular cross-section of the corroded bar, the average $\phi_{avg,c}$ and minimum $\phi_{min,c}$ residual diameter are directly calculated by the average and minimum residual cross-section. The average and maximum corrosion penetration p_{avg} and p_{max} are then estimated as the

Table 5 Estimate of the corrosion attack characteristics, definition of the parameters

Symbol	Unit	Definition	Equation	
K	mm/years$^{1/2}$	CO_2 penetration rate	$K = dCO_2/\sqrt{T_{survey} - T_{0,agg}}$	
T_i	years	corrosion initiation time	$T_i = cc^2/K^2$	
T_p	years	corrosion propagation time	$T_p = (T_{survey} - T_{0,agg}) - T_i$	
T_c	years	corrosion time	Estimated depending on the Scenario	
$\phi_{avg,c}$	mm	average corroded diameter	$\phi_{avg,c} = \sqrt{4 \cdot A_{avg,ts}/\pi}$	
$\phi_{min,c}$	mm	minimum corroded diameter	$\phi_{\min,c} = \sqrt{4 \cdot A_{\min,ts}/\pi}$	
p_{avg}	μm	average corrosion penetration	$p_{avg} = (\phi_0 - \phi_{avg,c})/2$	model 1
			$p_{avg} = \phi_0 - \phi_{avg,c}$	model 2
p_{max}	μm	maximum corrosion penetration	$p_{\max} = \phi_0 - \phi_{\min,c}$	
R_p	–	maximum to average corrosion attack ratio in terms of penetration	$R_p = p_{\max}/p_{avg}$	
v_{avg}	μm/year	average corrosion rate	$v_{avg} = p_{avg}/T_c$	

difference between the original diameter ϕ_0 and the equivalent diameter of the average corroded cross-section $\phi_{avg,c}$, and of the minimum corroded cross-section $\phi_{min,c}$, respectively. According to a simplified model proposed in the literature [6], the average corrosion penetration can be estimated by following two different models, among others (Model 1 and 2 in Fig. 6): in the former, the attack is considered as homogeneous on the bar section, and the diameter reduction is twice the corrosion penetration depth; in the latter, the corrosion attack occurs from one side of the bar and the corrosion attack penetration corresponds to the diameter reduction. Consequently, the average corrosion penetration (and the corrosion rate v_{avg}) obtained with model 2 is doubled with respect to the same obtained with model 1. The maximum to average attack ratio in terms of corrosion penetration R_p can finally be calculated; whereas the corrosion rate v_{avg} requires the definition of the corrosion time T_c, which can be equal or lower than the corrosion propagation time T_p. The corrosion propagation time is the difference between the structure age T_a and the corrosion initiation time T_i, where the structure age is assumed as the time frame from construction up to the date of the investigation (T_{survey}); the initiation time is the time frame from construction to the moment when aggressive substances (carbonation or chlorides) reach the rebar level (Equations in Table 5). In detail, for carbonation-induced corrosion, this can be preliminarily obtained by comparing carbonation depth with the concrete cover thickness. Indeed, by adopting Fick's second law of diffusion [23] to describe the penetration of carbonation in concrete, the CO_2 penetration rate K is first estimated by considering the depth of carbonation reached at the time of the survey (since the moment the structure was exposed to an aggressive environment, marked as $T_{o,agg}$, which often corresponds to time of construction), and then

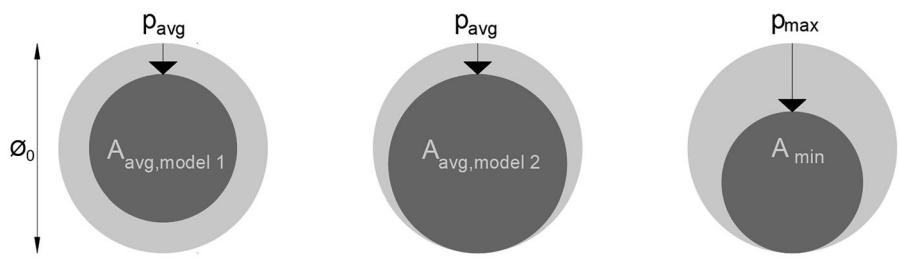

Fig. 6 Equivalent average and minimum residual cross-section for the corroded bars according to penetration obtained with model 1 (left) and model 2 (centre) [4]

applied to obtain a first rough estimation of the initiation time. After bars depassivation, in natural environments, corrosion rate is not constant over time, but it is characterised by daily and seasonal variation related to the micro-climatic and aggressive conditions in the concrete surrounding the bars. However, in order to estimate values of corrosion rates to be associated with the Scenarios, an average corrosion rate, constant over the corrosion time T_c is considered.

Results are presented in Table 6. While the corrosion attack distribution and its geometrical characteristics (Table 4) are obtained by the elaboration of the data resulting from the tomography and can be considered accurate, several assumptions were made to obtain an estimate of the corrosion attack characteristics of interest (reported in Table 6). The main parameters influencing the results are the definition of the initiation and effective corrosion time (related to the available information about the building history, the accuracy of in-field measurements of carbonation depth or chloride profile) and the model adopted for the calculation of corrosion penetration, which depends to the type of corrosion attack and the shape of the residual cross-section. In real structures, it is often difficult to estimate the approximated initiation time, due to the variability of both the concrete cover dimension and of the carbonation depth. However, for the case-study buildings, this information is not so relevant. For example, in the building AB (60 years at the time of the survey), where corrosion processes activated after the gutter collapsed (14 years before the survey), the possible variability in the duration of the initiation time (estimated as 18 years after construction) does not influence the calculation of the corrosion time. Also, when initiation time is estimated to be very close to year of construction, its influence on the corrosion rate's estimate decreases with the age of the structure (see for example the building RB), and so do the uncertainties related to this information. In chloride-induced corrosion (scenario 3), the propagation time usually corresponds to the corrosion time because, as the critical chloride threshold reaches the rebar level, an intense attack occurs, and the structural safety may be compromised. For bar IB1, although the estimated corrosion rate is very dependent on the definition of the propagation time, which is unknown, the corrosion rate results are very high compared to all the other scenarios, up to an order of magnitude, even when 10 years of active corrosion are considered.

As for corrosion penetration, Model 1 was chosen for those bars in which the attack was mainly triggered by the presence of chloride surrounding the bar; in the other cases, being water leakage and infiltration the main cause of corrosion, model 2 with the attack penetrating from one side of the bar was assumed. It is therefore worth noting that, the estimate of the average corrosion rate and of the maximum-to-average attack ratio, being both dependent on the average corrosion attack penetration, may be double or half of the proposed value, according to the selected model.

The parameter indicating the ratio between the maximum and average corrosion attack on the bar section has been herein expressed in terms of maximum corrosion attack penetration over the average

Table 6 Estimate of the corrosion attack characteristics, results

	T_a years	K mm/years^{-1}	T_i years	T_p years	T_c years	$\phi_{avg,c}$ mm	$\phi_{min,c}$ mm	Model –	R_p –	v_{avg} μm/year
AB1	60	6.8	8	52	0	–	–	–	–	–
AB2	60	5.9	18	42	14	15.60	15.31	2	1.72	28.6
AB3	60	5.9	18	42	14	15.70	15.47	2	1.76	21.4
AB4	60	5.9	18	42	14	15.58	15.19	2	1.93	30.0
RB1	50	5.7	7	43	43	18.97	17.95	2	1.98	24.0
RB2	50	8.5	3	47	47	15.68	15.57	2	1.36	6.8
SB1	61	12.8	7	54	54	9.59	8.76	1	4.33	6.6
SB2	61	11.5	15	46	46	8.94	7.44	1	5.49	9.3
IB1	30	n.a	n.a	n.a	2–10 (6)*	7.30	5.66	1	3.21	675–135 (225)

penetration ($R_p = p_{max}/p_{avg}$). This parameter R_p should be preferred to the maximum cross-section reduction over the average reduction ($R_{sec} = \Delta A_{max}/\Delta A_{avg}$) for the characterization of the Scenarios since the latter is also influenced by the bar original diameter. Val, (2007; [24]), in expressing the ratio between the maximum and average attack, suggest to the ratio between the maximum attack penetration in the pit (by modelling the actual pit shape) and the average attack penetration (by assuming a uniform attack). However, as far as the preliminary assessment of the existing structures residual capacity is concerned, difficulty may arise in defining the pit shape and consequently defining the actual dimension of the minimum residual cross-section in real applications.

Finally, the characteristics of the corrosion attack estimated in this work were compared to data found in the literature, in relation with average corrosion rates measured in several environmental conditions. Corrosion rates reported in the literature (referred as B—Bertolini, et al., 2013 [23]; MA—Martínez & Andrade, 2009 [9]; R—RILEM, 1996 [25]) and values from the current investigation (herein labelled E) are shown in Table 7. It is worth noting that the values of the corrosion rate measured in this work on existing structures match well to the intervals proposed in the literature. However, it is evident that the proposed value ranges are still too wide to be adopted in the practical applications and should be refined by extending the in-field data collection and inventory, to ensure a reliable stochastic database. As for the other characteristics of the Corrosion Scenarios to be defined (maximum to average attack ratio, attack distribution along the bar length), few data are available in the literature which can be associated with the Scenarios [26]. For this reason, the data collected can be used to draw some preliminary considerations on those parameters, although they cannot be used as a reference, for the limited number of samples analysed.

4 Effects of corrosion pattern on the mechanical behaviour of naturally corroded bars

The possible variation of the mechanical properties of naturally corroded bars was also investigated. The bars sampled from the existing buildings were subjected to tensile tests to determine their residual strength and ductility, and the results were related to their corrosion pattern. In order to investigate the relationship between the corrosion pattern on the bar and its mechanical behaviour, formulations are proposed in the literature, based on empirical equations or numerical models, aimed at defining a modified stress–strain relationship for the corroded bar. Among those, Cairns et al., 2005 [27] investigated the behaviour of bare bars with mechanical induced localized damage (simulating pitting corrosion) and of bars embedded in concrete subjected to artificial corrosion. It emerged that a strong reduction in ductility is noticed in presence of localized attacks, and that the effect on the yield strength (considered the main design parameter for bar resistance) are less significant. Imperatore et al., (2017 [28]) defined empirical relationship for the mechanical parameters of corroded bars as a function of the mass loss, starting from experimental tests on artificially corroded bars; Haefliger and Kaufmann, 2022 [8] investigated the behaviour of RC elements in tension with embedded locally corroded reinforcement, and proposed a modified tension chord model for structural analysis.

In the experimental investigations with artificially corroded bars, reference uncorroded samples are usually available and used to measure the initial mechanical properties. In this work, dealing with existing structures, an uncorroded reference bar portion was not always available, therefore the comparison was carried out, when possible, between the corroded bar and a reference smaller cross-section specimen obtained by smothering the corroded bar itself as to remove the outer corroded layer and obtain a sample with uncorroded steel and uniform cross-section distribution.

This operation may have led to a slight reduction in the strength of the reference specimens compared to that of the original bar, due to the removal of the outer layer of the bar cross-section. Depending on the manufacturing process and resulting steel microstructure, the effects of the outer layer removal can vary significantly in steel bars. The outer layer usually presents higher mechanical properties (in terms of strength) with respect to the inner core (which instead is characterized by higher ductility). This effect is likely to be modest for the examined bars since, in the past, the required mechanical properties were obtained through the use of a high carbon content, resulting in a slight difference between the characteristics of the

Table 7 Representative average values of the corrosion rate in each Corrosion Risk Scenario divided into three aggressiveness classes (O-Ordinary, H-high, E-Extreme). Values proposed in the literature: B [23], MA [9], R [25], E (estimated values from existing structures), T [26]

Scenario		S1	S2	S3
Corrosion phenomenon		Carbonation-induced corrosion	Carbonation-induced corrosion + Cl^-	Critical Cl^- threshold at rebar level
Average corrosion rate v_{avg} [μm/year]	**CLASS O** Ordinary R.H. (S2) or marine atmosphere (S3)		B: 2–10 E: 7 (0.20% Cl) 10 (0.34% Cl)	B: 10–50 MA: 4 R: 9–40
	CLASS H High R.H. (S1-S2), chloride airborne (S3)	B: 2–10 MA: 2 R: 1–12 E: 7	B: 10–100 E: 24 (0.27% Cl)	B: 50–100 MA: 30 R: 40–80
	CLASS E Alternation of very wet/dry environment (S1-S2) or zones of water stagnation, splash/tidal zone (S3)	B: 10–100 MA: 5 R: 12–50 E: 22–30	B: 100–200	B: 100–1000 MA: 70 R: 80–120 E: 220
Maximum to average attack ratio R_p		MA: 1 E: 1.3 ÷ 1.9	E: 2.0 ÷ 2.6	MA: 10 T: 4 ÷ 8 E: 1.6
Maximum attack type on the bar length		Portion of the bar	Localized deeper attacks	Pitting
Possible attack distribution on the bar length		Uniform	Spread with localized deeper attacks	Spread with deeper attacks or very localized

internal core and the outer layer; this effect is more pronounced for bars manufactured today by means of quenching and self-tempering processes [28]. The same considerations on the bar strength possible reduction hold for the effect of corrosion penetration since the attack largely involves the outer layer of the bar.

4.1 Specimen preparation and test procedure

Tensile tests were performed on all the sampled bars, except for IB1, being too short for a reliable test. Most of the tested bars segments were plain steel bars from the '60 s, with original diameter ranging between 16 ÷ 20 mm, probably manufactured by hot-rolling. The bars from the school building SB1-2 featured instead an original nominal diameter of 10 mm, being probably cold-drawn profiles.

Although the bars come from different structures and could be made of different types of steel, similarities in the measured properties, the periods of construction, and the fact that the bars are smooth, may indicate that the bars are made of the same type of steel, most likely AQ50 [29], with yield strength $f_{yk} > 270$ MPa, tensile strength f_{tk} ranging between 500 ÷ 600 MPa, and percentage elongation after fracture (i.e. the elongation measured after the test with respect to a reference length, expressed as a percentage of the length itself) $A > 16\%$ [30]. The tensile tests were carried out on corroded bars extracted from the buildings and on reference specimens according to EN ISO 15630–1 [22] and EN ISO 6892–1 [31], respectively. All the samples were subjected to monotonic tensile tests up to failure, conducted in displacement control.

4.1.1 Tensile tests on reference specimens

Reference specimens were prepared according to Annex D in EN ISO 6892–1 [31], and symbology adopted accordingly. The uniform cross-section of the reference specimen (S_0) was chosen imposing to be smaller than the minimum section of the corroded bar, in order to obtain a sample with uniform cross-section distribution, not affected by corrosion. The reference length for elongation measurement (L_0) was marked on the sample before the test; the distance between marks was measured at the end of the test (L_u). The elongation after fracture A of each sample was measured as $A = (L_u\text{-}L_0)/L_0$.

4.1.2 Tensile tests on corroded bars

As for the corroded bars, failure always occurred at the bars' weakest sections, characterized by the cross-section A_{min} (Table 4). Therefore, the effective stress reported in Fig. 7 is calculated as the axial tensile force (N) recorded during the test divided by this value ($\sigma = N/A_{min}$). The same plot is reported by considering the nominal stress, that is obtained by dividing the axial load for the nominal cross-section ($\sigma = N/A_0$; Fig. 8). As for the conventional strain ε^* reported in x-axis, the relative displacement between bar anchorages over the bar length is considered. It should be noted that such measurements can provide information about the behaviour of the bar, but it cannot be used to determine the correct elongation (and consequently the actual strain during the test) because of the possible slippage of bar anchorages. The actual strain is thus smaller than the registered conventional strain ε^* and can be only locally determined by strain gauges (by smoothing the bar surface and gluing them on it, thus altering the residual cross-section distribution) or by an extensometer. However, neither of these two methods provide significant information in the case of corroded bars, referring only to the portion of the bar in which they are applied and therefore being not suitable for bars with uneven cross-section distribution. Due to the absence of such measurements, the stiffness of the bar in the elastic branch cannot be accurately determined. For the analysed bars, an estimate of the ductility reduction was therefore obtained through the manual method, by measuring the elongation after fracture (as for the reference specimens); equidistant marks at 10 mm intervals were made before the test, along the whole bar length. The percentage elongation $A(\%)$ was then measured after the test on a reference gauge length L_0 = 100 mm, at a distance of the largest

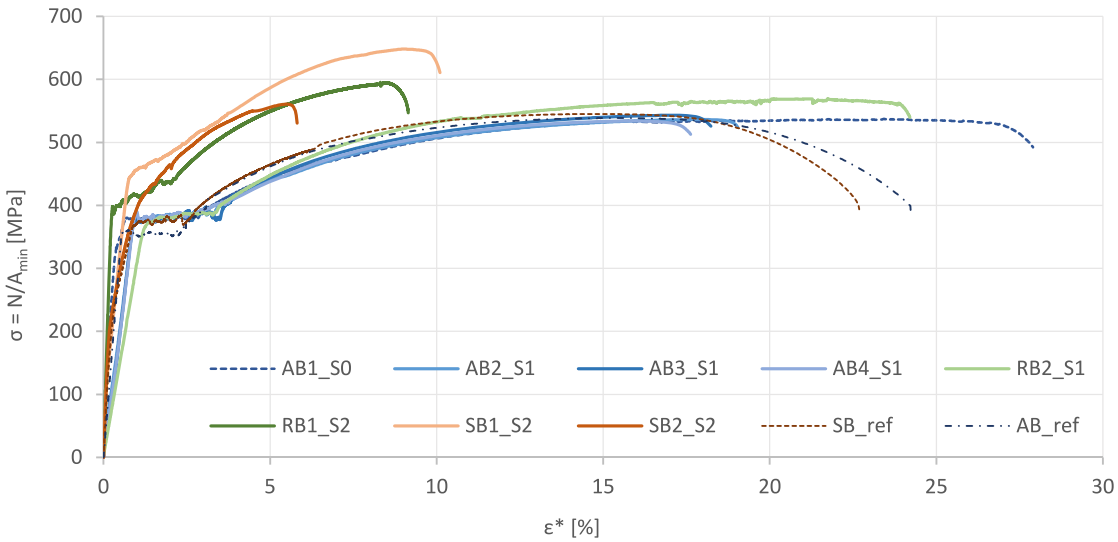

Fig. 7 Comparison of stress–strain plots obtained for different bars by dividing the applied load N for the minimum cross-section of the bar. The strain ε** reported in x-axis is the relative displacement between bar anchorages divided by the bar initial length. Gradation of the same colour is assigned to bar belonging to the same building; CRS of reference is reported in the legend (S0-1-2-3)

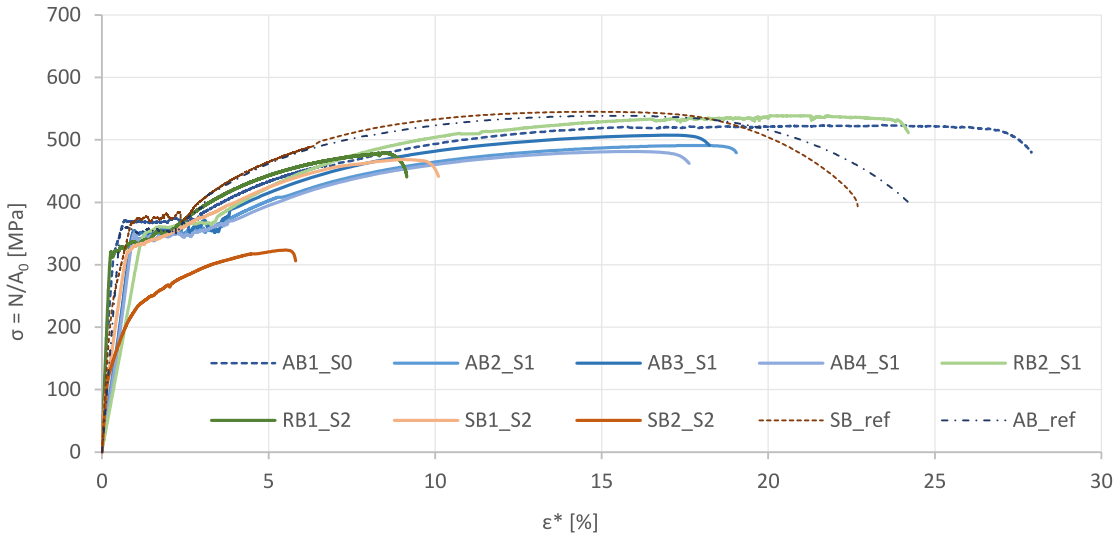

Fig. 8 Comparison of stress–strain plots obtained for different bars by dividing the applied load for the initial nominal cross-section of the bar. The strain ε* reported in x-axis is the relative displacement between bar anchorages divided by the bar initial length. Colours and legend as in Fig. 7

Table 8 Tensile tests results

Extracted bars	$L_{0,bar}$ [mm]	Φ_0 [mm]	$A_{min,ts}$ [mm^2]	F_y [kN]	F_m [kN]	$f_{y,nom}$ [MPa]	$f_{u,nom}$ [MPa]	$f_{y,min}$ [MPa]	$f_{u,min}$ [MPa]	L_0 [mm]	L_u [mm]	A [%]
AB1	290	15.9	193.6	73.3	106.1	367	534	377	548	100.0	118.1	18.1
AB2	379	16	184.1	68.0	100.8	338	501	369	548	100.0	111.5	11.5
AB3	367	16	187.9	71.0	102.0	353	507	378	543	100.0	112.6	12.6
AB4	366	16	181.3	69.6	98.8	346	492	384	545	100.0	113.8	13.8
RB1	485	20	253.2	98.9	150.7	315	480	391	595	100.0	107.5	7.5
RB2	400	16	190.4	69.9	108.3	348	539	367	569	100.0	116.0	16.0
(SB1)	325	10.3	60.2	26.2	39.7	314	476	435	659	50.0	54.1	8.2
SB2	200	9.8	43.5	8.0	25.0	106	331	183	574	50.0	51.5	3.0
Ref. Specimen	$L_{0,bar}$ [mm]	Φ_0 [mm]	S_0 [mm^2]	F_y [kN]	F_m [kN]	$f_{y,nom}$ [MPa]	$f_{u,nom}$ [MPa]	$f_{y,min}$ [MPa]	$f_{u,min}$ [MPa]	L_0 [mm]	L_u [mm]	A [%]
AB_ref	78	12.3	118.8	41.9	64.0	353	539	353	539	60.0	76.7	27.8
SB_ref	40	5.65	25.1	9.2	13.9	367	553	367	553	25.0	33.2	32.8

measurement between 50 mm and two diameters away from the fracture [22].

4.2 Tensile test results

The results of the tensile tests are reported in Table 8 and the stress-conventional strain relationship is compared for all the tested samples in Fig. 7,8. Reference specimens were prepared for the sole groups of bar AB (AB_ref) and SB (SB_ref). For the abandoned building, the uncorroded bar AB1 (Scenario 0) was also tested, and the results were compared with the corroded bars removed from the same building (AB2-3–4 in Scenario 1). Since it was not possible to obtain a reference specimen for bars RB1-RB2, the reduction of the mechanical properties of the bar RB1 was estimated by comparing its behaviour with that of bar RB2, sampled from the same building,

and only slightly corroded. Finally, the failure location for bar SB1 was inside the anchorage and for this reason the test may not be considered valid. Considering the residual cross-section profile of the sampled bars reported in Fig. 5, it should be noticed that some portions of the bars were removed before testing, either to have similar length among tested bars from the same building or to prepare reference specimens. Following portions were removed: a length of 176 mm from the left in bar AB2; 100 mm from each side in bar AB4 and 120 mm from the left in bar SB2. In Table 8, the resulting length between anchorages is reported for each tested bar ($L_{0,bar}$).

Considering the bars from the building AB, the plots in Fig. 7 show that, when the stress is calculated by dividing the applied load for the minimum cross-section A_{min}, the yielding stress in the corroded bars (AB2-3–4) and the uncorroded bar (AB1) match well. The four stress–strain plots are almost coincident in term of strength values. Slightly higher values of yielding stress are measured in these bars with respect to the reference specimen AB_ref (Table 8). As anticipated, this could be due to the removal of the outer layer in AB_ref, due to the smoothering process. On the other hand, a reduction in the elongation capacity of the corroded bars with respect to the uncorroded one is evident from the value of A (%) reported in Table 8, about 12.5% compared to 18%. The result highlights a reduction of the elongation capacity which is very similar among the corroded bars presenting similar corrosion attack patterns. Therefore, a reduction of the elongation capacity of the corroded bar in tension can be expected even when very localized attacks are not present, due to the uneven residual cross-section distribution along the bar length [5]. When considering the nominal stress (Fig. 8), the reduction in the yield strength (the average value for corroded bars AB is 345 MPa) with respect to the original bar is between 0% ÷ 4% or 6% ÷ 10% if comparison is made with the reference specimen AB_ref or with the bar AB1, respectively. A reduction of the nominal maximum strength between 6% ÷ 10% is instead observed regardless of the sample considered for reference. The reduction in term of strength is thus very similar to the maximum cross-section reduction (6% ÷ 10%).

As for the building RB, the behaviour of the two bars, in term of yielding (f_y) and ultimate (f_u) stresses, is comparable; in this case, not having a reference specimen available, the most relevant data is the strong reduction in the elongation capacity observed for bar RB1 (A = 7.5% for RB1 and A = 16% for RB2), due to the significant cross-section reduction over a limited length of almost 200 mm (Fig. 5b).

As for bars SB1 and SB2, characterized by severe pitting attacks, a strong reduction in ductility is noticed with respect to the reference sample (SB_ref); in this case, considering the effective stresses (Fig. 7), a sharper difference is observed between the higher stresses (at same deformation) measured in the corroded bar with respect to the reference sample. These two bars are the sole characterized by a cold-drawn profile manufacturing, therefore the difference between the mechanical properties of the bar core and the outer layer are probably more pronounced with respect to the other hot-rolled bars, thus the removal of the outer layer may have led to a higher reduction of the reference specimen (SB_ref) strength. A clear yielding point was not detected for bar SB2. Also, the possibility of achieving a higher maximum strength during tensile tests could be limited by the ductility reduction. Finally, the comparison between the nominal stresses in the reference sample SB_ref and in the corroded bars shows a lower reduction of maximum strength with respect to the maximum cross-section reduction (14% with respect to 27% for bar SB1, 40% with respect to 46% for bar SB2).

4.3 Considerations on the mechanical behaviour of corroded bars

The tests carried out on the selected naturally corroded bars show that the reduction in capacity (both yielding and maximum strength) seems to be related mostly to the maximum reduction of the bar cross-section, at least for the smooth bars tested in this investigation. In case differences in the microstructure of the bar cross-section are present, or differences between the mechanical properties of the outer layer and of the inner core are present, a further reduction of the bar capacity may be expected.

On the other hand, a significant reduction of the elongation capacity of the corroded bars is observed, especially in the case of localized attacks (Scenario 2). The heaviest loss in elongation capacity was observed in SB1 and SB2, where the typical pitting attack occurred, and in RB1, where a severe cross-section reduction of 20% extended over a length of almost

200 mm at the bar centre (much higher than the average reduction of about 10%).

As for the bars sampled from the abandoned building (AB), a reduction in ductility is also observed, but it is less pronounced. Based on the above, it can be observed that, for the bars analysed in this study, a reduction in the elongation capacity may occur for all the Corrosion Risk Scenarios, provided that the residual cross-section profile along the bar is not homogeneous. Nevertheless, the relevance of such elongation capacity reduction in the global structural behaviour should be further investigated.

In Table 9 and Figs. 9, 10 the percentage elongation (A) (measured in all the tested bars using the manual method) is reported as a function of the maximum attack occurring in the minimum residual sections of the bars, which can be expressed as either the ratio of the minimum cross-section over the original one (A_{min}/A_0, Fig. 9a) or as the ratio of the maximum cross-section reduction over the original section ($\Delta A_{max}/A_0$). The latter graph is reported for the sake of comparison with a widely used empirical expression [32], which describes a linear decreasing trend between the residual ultimate strain of a corroded bar and $\alpha_{PIT} = \Delta A_{max}/A_0$, that is the area reduction due to pitting over the original cross-section. Considering the bars tested in this experimental program, the reduction in ultimate strain is here expressed in terms of A *[%];* the ultimate strain is defined as the one of the virgin material (associated with A *[%]* = 18.1, corresponding to the uncorroded bar AB1), if the attack is not present, and with the yielding strain (associated with A *[%]* = 0) if $\alpha_{PIT} = \alpha_{PIT}^{MAX}$. Values of α_{PIT}^{MAX} ranging between 0.1 ÷ 0.5 were proposed in the literature. In Fig. 9b it is observed that the results are compliant with the proposed trends [32]. Furthermore, given that the elongation capacity also depends on the corrosion attack variability and distribution along the length of the bar, the elongation capacity is also reported as a function of the ratio of the cross-section range over the average cross-section ($\Delta A_{ts}/A_{avg}$ where $\Delta A_{ts} = A_{max,ts} - A_{min,ts}$, Fig. 10a and the coefficient of variation ($Co.V. = st.dev/A_{avg}$ where $st.dev$ is the standard deviation, Fig. 10b). Although a clear trend cannot be identified based on the few data available from this investigation, it appears that the larger the range and the coefficient of variation, the lower the elongation capacity.

5 Research contributions and research needs

This paper focused on the characteristics of corrosion attacks expected in natural environments and on their effects on steel bars, both in terms of residual cross-section distribution and reduction in mechanical properties, such as strength and ductility. These data are, at the same time, fundamental to calibrate any further structural model for the assessment of corroded RC structures, and rarely available. Due to such a limited knowledge, in-field surveys and experimental tests were performed on few existing structures exposed to different environmental conditions. First promising results were obtained regarding the possibility of establishing a relationship between the environmental and aggressiveness conditions and the main characteristics of the corrosion attack, in terms of intensity and pattern. The Corrosion Risk Scenarios (CRSs) proposed by the authors in the DEMSA Protocol [4] were considered as a reference to classify such environmental conditions.

For each sampled bar, the corrosion pattern on the bar surface was analysed, and possible variation of

Table 9 A [%] in relation to the minimum cross-section with respect to the original and to the cross-section range with respect to the average section

Bar #	AB1	AB2	AB3	AB4	RB1	RB2	SB1	SB2
A [%]	18.1	11.5	12.6	13.8	7.5	16.0	8.2	3.0
A_{min}/A_0 [%]	97.0	91.6	93.5	90.2	80.6	94.7	72.3	57.7
α_{PIT}	0.03	0.08	0.07	0.10	0.19	0.05	0.28	0.42
$\Delta A_{ts}/A_{avg}$ [%]	2.2	7.0	4.9	6.9	16.4	3.7	30.5	50.5
cv [%]	0.3	1.2	0.9	1.7	3.9	0.6	7.0	16.8

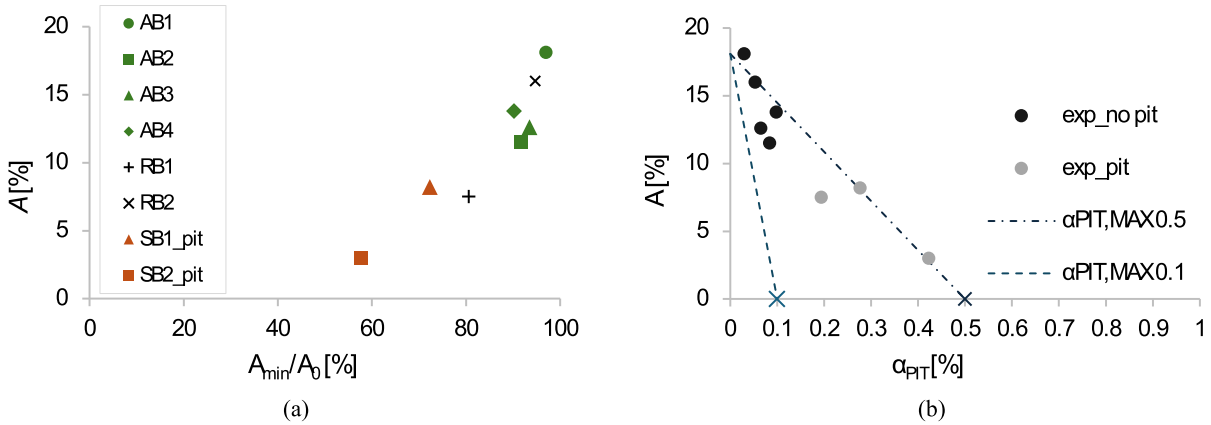

Fig. 9 Percentage elongation after fracture A [%] for the tested bars in relation to the maximum corrosion attack, expressed as the minimum cross-section (**a**) or the maximum cross-section reduction (**b**) over the original. exp_no pit: referred to bars with no pitting or localized attack (AB1, AB2, AB3, AB4, RB2); exp_pit: referred to bars with pitting (SB1, SB2) or localized attack (RB1)

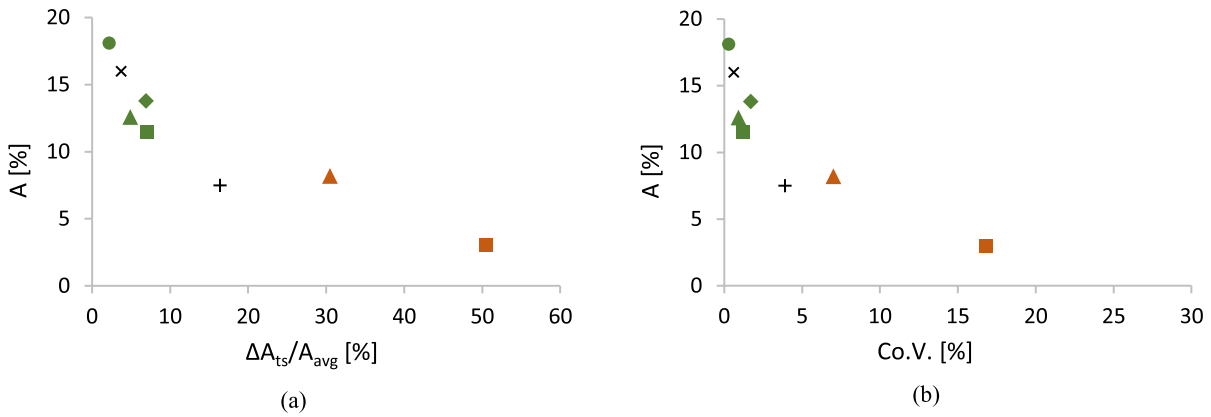

Fig. 10 Percentage elongation after fracture A [%] for the tested bars in relation to the range over the averagecross-section (**a**) and to the coefficient of variation of the cross-section distribution (**b**). Legend as in Figure 9a.

mechanical properties investigated. Beside chloride-induced corrosion is acknowledged as to produce the heaviest effects on bars and structural elements (also confirmed by the analysis of the bar IB1 in Scenario 3), the examples presented in this paper highlight that also Scenario 1 (carbonation and high R.H. or frequent wet/dry cycles) and 2 (carbonation and low chloride content) need to be considered when dealing with existing RC structures because relevant attacks for the structural behaviour can be found. The attack in Scenario 1 may induce a generalized reduction of the bar cross-section, significant production of oxides along the whole bar length and consequently possible concrete spalling/delamination and reduction in bond-strength; in Scenario 2, localized attack may occur with minor external signs of damage with respect to heavy chloride-induced corrosion.

Considering the relationship between the corrosion attack and the CRS, it was observed that, by increasing the Scenario (from 1 to 3) and the aggressiveness class, a more intense and uneven attack is expected, due to the higher chloride content and relative humidity. In case of carbonation-induced corrosion (Scenario 1), a more uniform attack is measured, although the maximum to average attack ratio can rise to $R_p = 2$, differently from that proposed in the literature (always assumed as $R_p = 1$). In presence of chlorides (Scenario 2–3), a smaller minimum residual cross-section, and a higher variability of the attack (here described by the cross-section range and coefficient of variation) is

found; also in this case, the definition of the maximum to average attack ratio requires more research, since very different values were found, with respect to the reference of $4 \div 10$ proposed in the literature. For the examined bars, the estimated values of the average corrosion rate v_{avg} ($10 \div 50$ µm/year for Scenario 1 and 2, higher than 100 µm/year for Scenario 3), well matched with the ranges proposed in the literature, which, however, should be improved and refined to be used in practical applications.

As for the plain bars analysed, the reduction in strength is mostly related to the cross-section reduction; therefore, for a preliminary analysis, it can be estimated by defining the average corrosion rate, the maximum to average attack ratio, the corrosion duration and the model for the residual cross-section shape. The tensile tests carried out showed that a reduction in ductility is always observed as far as the attack distribution along the bar length is variable. Therefore, simplified parameters describing the attack variability along the bar length should be defined. A possible approach, requiring further research, is proposed by the authors in Casprini et al., 2022 [5]. Finally, the parameters describing the corrosion effects on the bars and on the surrounding concrete can be implemented in structural analysis to estimate the residual strength and ductility of structural elements, and the modified behaviour of the whole structure, which is the final aim of the assessment procedure.

Acknowledgements The authors wish to acknowledge the precious collaboration of Matteo Gastaldi (Politecnico of Milan) for the support provided in corrosion processes, material engineering, and chemical analyses; the authors are grateful to Paolo Riva, Ezio Giuriani, and the municipality of Brescia for the possibility of working on real case-studies. In-field and laboratory tests were carried out with the fundamental support of Laboratorio Prove Materiali (University of Bergamo), Laboratorio Strutture (University of Florence), Elena Crotti, and Leonardo Bucci. Tomographic scan results were provided by TEC Eurolab Srl (Modena, Italy), whose proficiency is gratefully acknowledged. The authors wish to thank the reviewers for their valuable suggestions, which have significantly improved the quality of the manuscript.

Funding Open access funding provided by Università degli studi di Bergamo within the CRUI-CARE Agreement.

Declarations

Conflict of interest The authors declare no conflict of interest. This research received no external funding. The authors have no financial or proprietary interests in any material discussed in this article.

Appendix 1

In the following figures, more detailed information about the bars extracted from the buildings described in this paper are reported. For each bar, four different visualizations of the external surface obtained through tomographic scans are reported, along with the shape of some significant cross-sections, and the residual area in percentage with respect to the original cross-section.

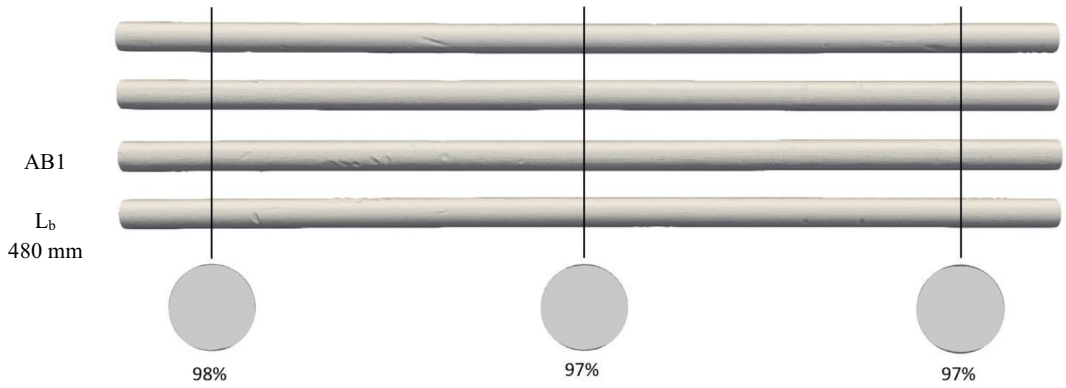
AB1
L_b
480 mm
98%
97%
97%

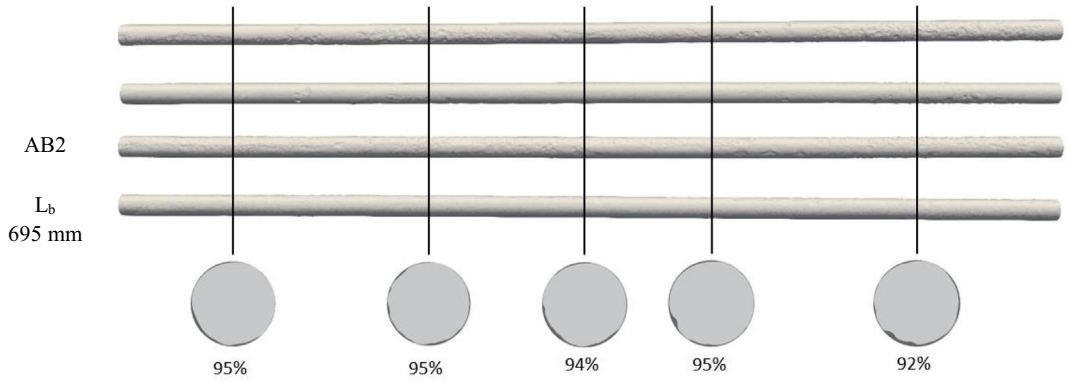
AB2
L_b
695 mm
95%
95%
94%
95%
92%

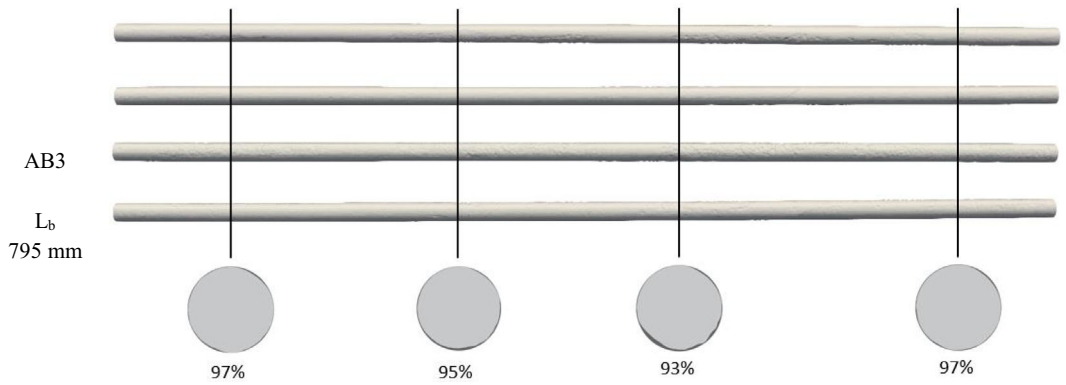
AB3
L_b
795 mm
97%
95%
93%
97%

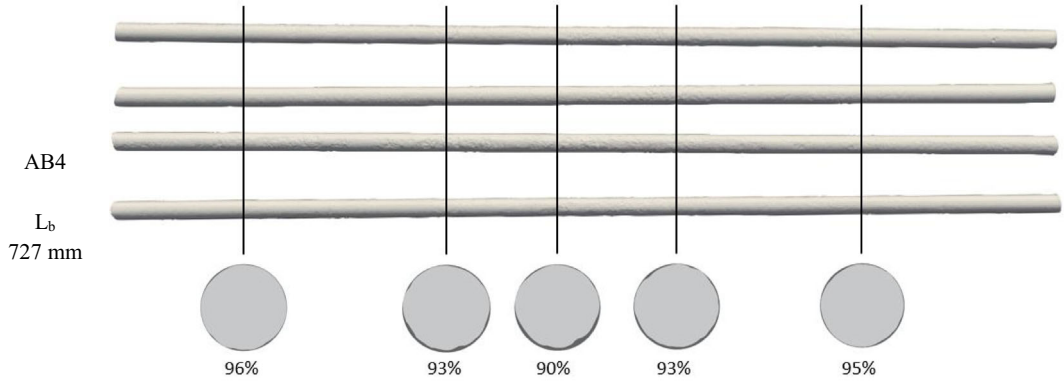
AB4
L_b
727 mm
96%
93%
90%
93%
95%

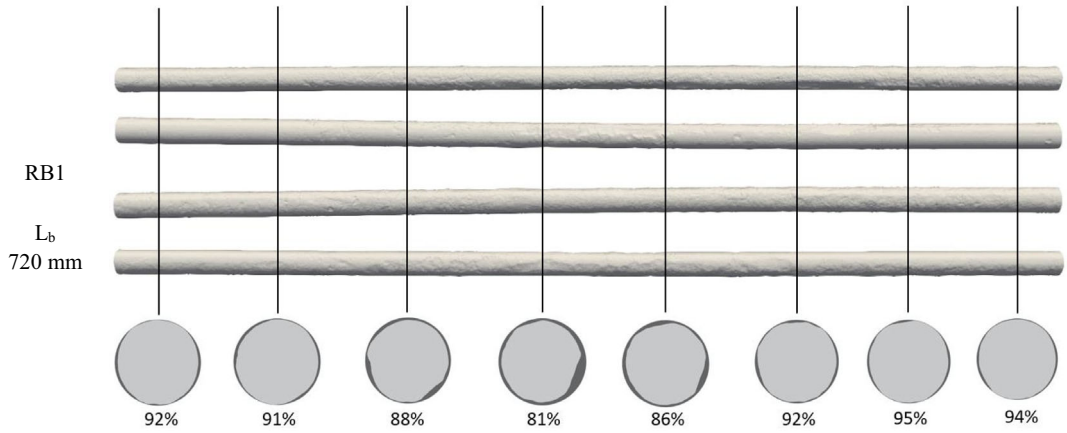
RB1
L_b
720 mm
92%
91%
88%
81%
86%
92%
95%
94%

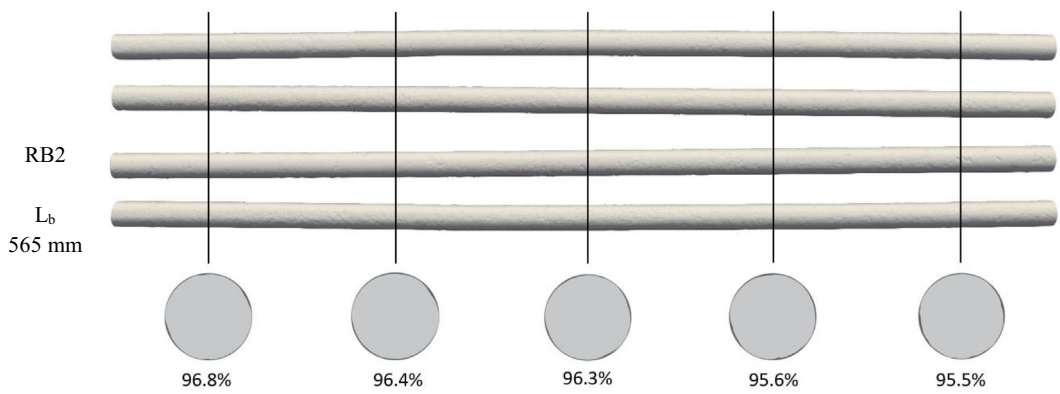
RB2
L_b
565 mm
96.8%
96.4%
96.3%
95.6%
95.5%

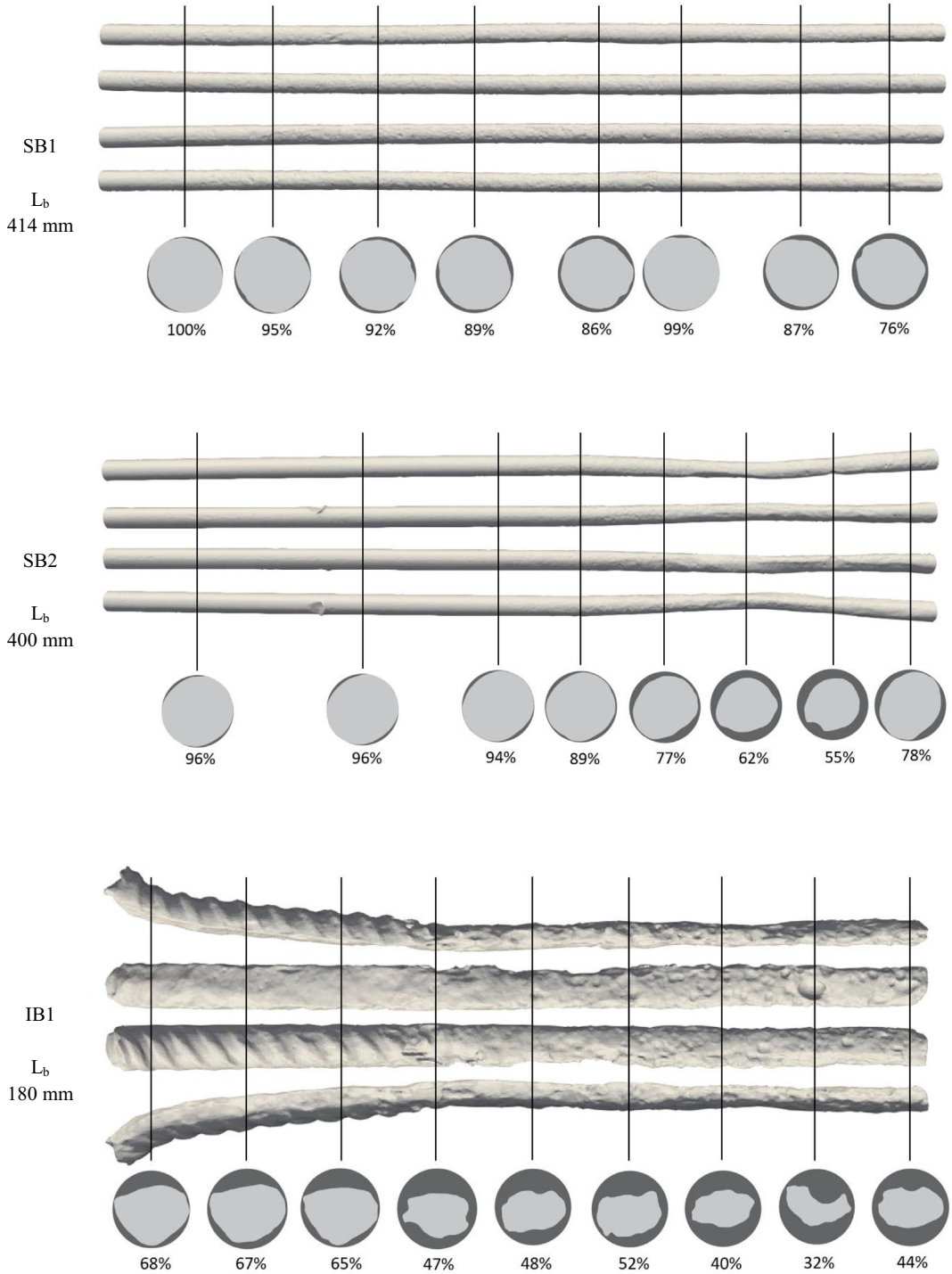
SB1
L_b
414 mm
100%
95%
92%
89%
86%
99%
87%
76%
SB2
L_b
400 mm
96%
96%
94%
89%
77%
62%
55%
78%
IB1
L_b
180 mm
68%
67%
65%
47%
48%
52%
40%
32%
44%

References

1. Rodríguez J (2023) New version of Eurocode 2: what is covered for the corroded concrete structures and how to be enlarged for an appropriate structural evaluation. Capacity Assessment of Reinforced Concrete Structures. Proceedings of the FIB Cacrcs days 2023
2. Di Carlo F, Meda A, Rinaldi Z (2023) Structural performance of corroded R.C. beams. Eng Struct 274:115117
3. Coronelli D, François R, Dang H, Zhu W (2019) Strength of corroded RC beams with bond deterioration. J struct eng (United States) 145(10):04019097
4. Casprini E, Passoni C, Marini A, Bartoli G (2022) DEMSA Protocol: deterioration effect modelling for structural assessment of RC buildings. Buildings 12(5):574. https://doi.org/10.3390/buildings12050574
5. Casprini E, Passoni C, Marini A, Bartoli G (2022) Toward the definition of equivalent damage parameters for the assessment of corroded RC structures. Struct Concr 24(1):11–24. https://doi.org/10.1002/suco.202200368
6. CONTECVET. IN30902I (2001) A validated user manual for assessing the residual life of concrete structures. DG Enterprise, CEC, 2001. https://www.ietcc.csic.es/wp-content/uploads/1989/02/manual_contecvet_ingles.pdf
7. Franceschini L, Belletti B, Tondolo F, Sanchez Montero J (2022) A simplified stress-strain relationship for the mechanical behaviour of corroded prestressing strand: the SCPS-model. Struct Concr 2022
8. Haefliger S, Kaufmann W (2022) Corroded tension chord model: load-deformation behaviour of structures with locally corroded reinforcement. Struct Concr 23(1):104–120. https://doi.org/10.1002/suco.202100165
9. Martínez I, Andrade C (2009) Examples of reinforcement corrosion monitoring by embedded sensors in concrete structures. Cement Concr Compos 31(8):545–554
10. Leporace-Guimil B, Russo N, Lollini F, Conforti A (2023) Morphological and mechanical characterization of reinforcement in cracked elements exposed to chloride-induced corrosion. Constr Build Mater 364:129822
11. Chen E, Berrocal CG, Fernandez I, Löfgren I, Lundgren K (2020) Assessment of the mechanical behaviour of reinforcement bars with localised pitting corrosion by digital image correlation. Eng Struct 219:110936
12. Caprili S, Mattei F, Salvatore W, Agostini M (2023) Analysis of corrosion effects on strands of prestressed concrete bridges with post-tensioned cables. Capacity assessment of reinforced concrete Structures. Proceedings of the FIB Cacrcs days 2023.
13. Palsson R, Mirza M. S (2002) Mechanical response of corroded steel reinfrocement of abandoned concrete bridge. ACI Structural journal
14. Fernandez I, Berrocal C G (2019) Mechanical properties of 30 year-old naturally corroded steel reinforcing bars. Int J Concrete Struct Mater https://doi.org/10.1186/s40069-018-0308-x
15. Marini A, Passoni C, Belleri A, Feroldi F, Preti M, Metelli G, Riva P, Giuriani E, Plizzari G (2017) Combining seismic retrofit with energy refurbishment for the sustainable renovation of RC buildings: a proof of concept. Eur J Environ Civ Eng 10:1080
16. Passoni C, Marini A, Belleri A, Menna C (2021) Redefining the concept of sustainable renovation of buildings: state of the art and LCT-based design framework. Sustainable Cities and Society, 64.
17. Casprini E (2021) A Protocol for the Assessment of Corrosion Effects in RC Structures in a life cycle engineering framework. Ph.D. Thesis, University of Bergamo, Dalmine, Italy.
18. EN 14269 (2007) Products and systems for the protection and repair of concrete structures—Test methods—Determination of chloride content in hardened concrete.
19. Felicetti R (2009). Improved procedure for the analysis of construction materials and device to implement this procedure. Italian Patent Application MI2009A 001073
20. Fernandez I, Lundgren K, Zandi K (2018) Evaluation of corrosion level of naturally corroded bars using different cleaning methods, computed tomography, and 3D optical scanning. Mater Struct, 51
21. Orobix Srl, Vmtk. The vascular modeling toolkit. Supported by Orobix srl. www.vmtk.org.
22. EN ISO 15630-1, 2002. Steel for the reinforcement and prestressing of concrete: test methods—Part 1: Reinforcing bars, wire rod and wire
23. Bertolini L, Elsener B, Pedeferri P, Redaelli E, Polder R (2013) Corrosion of Steel in Concrete—Prevention, Diagnosis, Repair; Wiley VCH: Weinheim, Germany.
24. Val DV (2007) Deterioration of strength of RC beams due to corrosion and its influence on beam reliability. J Struct Eng 133(9):1297–1306
25. RILEM (1996) Durability Design of Concrete Structures. Report No. 14. E&FN Spon: London, UK.
26. Tuutti K (1982) Corrosion of steel in concrete. Stockholm: Swedish cement and concrete research institute
27. Cairns J, Plizzari G, Du Y, Law D W, Franzoni C (2005) Mechanical properties of corrosion-damaged reinforcement. ACI Mater J 102(4)
28. Imperatore S, Rinaldi Z, Drago C (2017) Degradation relationship for the mechanical properties of corroded steel rebars. Constr Build Mater 148:219–230
29. LL. PP (1957) CIRCOLARE 23/05/1957 N° 1472. Armature delle strutture in cemento armato.
30. Verderame GM, Ricci P, Esposito M, Sansiviero FC (2011) Le caratteristiche meccaniche degli acciai impiegati nelle strutture in C.A. realizzate dal 1950 al 1980. Padova, 19–21 Maggio. Paper 54.
31. EN ISO 6892-1 (2016) Metallic materials -Tensile testing—Part 1: method of test at room temperature.
32. Coronelli D, Gambarova PG (2004) Structural assessment of corroding R/C beams: modelling guidelines. ASCE J Struct Eng 130:1214–1224